Dissecting the Intimate Mechanism of Cyanation of {2Fe3S} Complexes Related to the Active Site of All-Iron Hydrogenases by DFT Analysis of Energetics, Transition States, Intermediates and Products in the Carbonyl Substitution Pathway

Giuseppe Zampella,[a] Maurizio Bruschi,[b] Piercarlo Fantucci,[a] Mathieu Razavet,[c] Christopher J. Pickett,*[c] and Luca De Gioia*[a]

Abstract: A bridging carbonyl intermediate with key structural elements of the diiron sub-site of all-iron hydrogenase has been experimentally observed in the CN/CO substitution pathway of the {2Fe3S} carbonyl precursor, $[Fe_2(CO)_5\{MeSCH_2C(Me)(CH_2S)_2\}]$. Herein we have used density functional theory (DFT) to dissect the overall substitution pathway in terms of the energetics and the structures of transition states, intermediates and products. We show that the formation of bridging CO transitions states is explicitly involved in the intimate mechanism of dicyanation. The enhanced rate of monocyanation of {2Fe3S} over the {2Fe2S} species $[Fe_2(CO)_6\{CH_2(CH_2S)_2\}]$ is found to rest with the ability of the thioether ligand to both stabilise a μ-CO transition state and act as a good leaving group. In contrast, the second cyanation step of the {2Fe3S} species is kinetically slower than for the {2Fe2S} monocyanide because the Fe2 atom is deactivated by coordination of the electron-donating thioether group. In addition, hindered rotation and the reaction coordinate of the approaching CN^- group, are other factors which explain reactivity differences in {2Fe2S} and {2Fe3S} systems. The intermediate species formed in the second cyanation step of {2Fe3S} species is a μ-CO species, confirming the structural assignment made on the basis of FT-IR data (S. J. George, Z. Cui, M. Razavet, C. J. Pickett, *Chem. Eur. J.* **2002**, *8*, 4037–4046). In support of this we find that computed and experimental IR frequencies of structurally characterised {2Fe3S} species *and* those of the bridging carbonyl intermediate are in excellent agreement. In a wider context, the study may provide some insight into the reactivity of dinuclear systems in which neighbouring group on-off coordination plays a role in substitution pathways.

Keywords: bioinorganic chemistry · carbonyl ligands · density functional calculations · hydrogenases · iron

Introduction

X-ray crystallographic structures of Fe-only hydrogenases from *Desulfovibrio desulfuricans*[1] and *Clostridium pasteurianum*,[2] together with spectroscopic data on Fe-only hydrogenase from *Desulfovibrio vulgaris*,[3] show that the H-cluster, the active site at which protons are reduced to dihydrogen, is a conventional $\{Fe_4S_4\}$ cluster linked by a bridging cysteinyl sulfur group to an "organometallic" {2Fe3S} subsite (Figure 1). At the sub-site a terminal carbon monoxide, a bridging carbon monoxide and a cyanide ligand are bound at each iron atom, which also share two bridging sulfur ligands of a 1,3-propanedithiolate or possibly the related di(thiomethyl)amine unit. The Fe atom distal to the $\{Fe_4S_4\}$ cluster has a coordinated water molecule (or vacancy) in the resting paramagnetic oxidised state of the enzyme $\{H_{ox}\}$,

[a] Dr. G. Zampella, Prof. P. Fantucci, Prof. L. De Gioia
Department of Biotechnology and Biosciences
University of Milano-Bicocca
Piazza della Scienza 2 20126-Milan (Italy)
Fax: (+39) 02-644-83478
E-mail: luca.degioia@unimib.it

[b] Dr. M. Bruschi
Department of Environmental Science
University of Milano-Bicocca
Piazza della Scienza 1 20126-Milan (Italy)

[c] Dr. M. Razavet, Prof. C. J. Pickett
Department of Biological Chemistry, John Innes Center Norwich
NR4 7UH (UK)
Fax: (+44) 1603-450-018
E-mail: chris.pickett@bbsrc.ac.uk

 DOI: 10.1002/chem.200400442

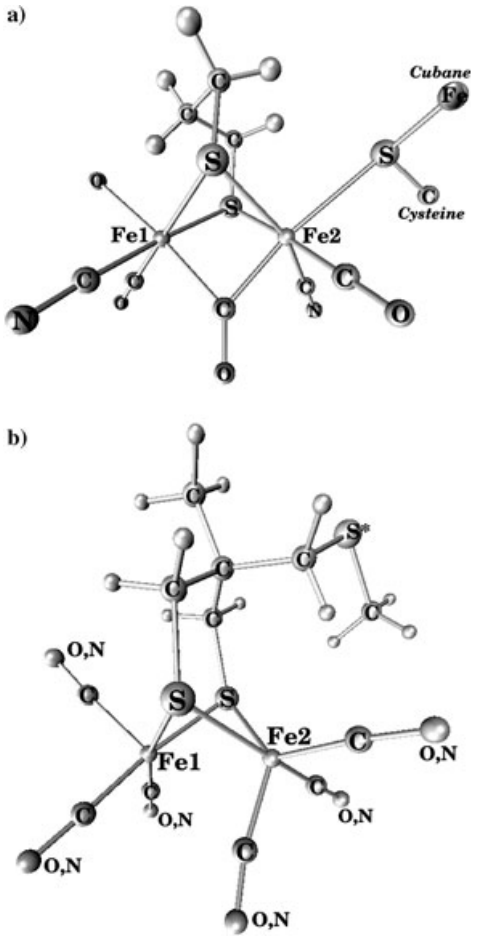

Figure 1. a) Proposed structure of the bimetallic cluster of Fe-only hydrogenases; this is a composite model combining features reported in reference [1] and [2]. The chelating disulfide ligand has been shown as 1,3-propanedithiolate but X-ray data are compatible also with a related azapropanedithiolate unit. b) Schematic representation of the class of {2Fe3S} models investigated in the present work. The thiother sulfur atom is labeled with * to denote that in some models this atom is coordinated to Fe2.

whilst carbon monoxide occupies this site in the CO-inhibited form of the enzyme.

The unusual structure of the sub-site has stimulated investigations aimed at shedding light on its structural, electronic and catalytic properties.[4–21] The sub-site resembles well-studied organometallic $Fe^{I}Fe^{I}$ complexes of the type $[(\mu\text{-}RS)_2Fe_2(CO)_6]$ (R = bridging organic group)[22,23] and such complexes provide precursors to di-cyanide derivatives such as $[Fe_2(CO)_4(CN)_2\{CH_2(CH_2S)_2\}]^{2-}$,[8–10] which is related to the structure of the CO-inhibited sub-site but lacks both differential S ligation and a bridging carbonyl ligand, as observed in the enzyme. The synthesis of model compounds even more closely related to the enzymatic subsite has been recently reported by Pickett and co-workers,[15,24] which have shown that the backbone modification of a propane dithiolate ligand can lead to {2Fe3S} species (Figure 1). In particular, the initial reaction of the molecule $[Fe_2(CO)_5\{MeSCH_2C(Me)(CH_2S)_2\}]$ (**A**) with cyanide takes place *regioselectively* at the Fe atom distal to the thioether ligand to give $[Fe_2(CO)_5(CN)(MeSCH_2C(Me)(CH_2S)_2)]^{1-}$ (**B**; Scheme 1), in which the thioether has dissociated from the iron center. Reversible dissociation of CO from **B** leads to the {2Fe3S} species $[Fe_2(CO)_4(CN)\{MeSCH_2C(Me)(CH_2S)_2\}]^{1-}$ (**C**). Subsequent reaction of **C** with cyanide results in the formation of a dicyanide species which has been spectroscopically characterised as $[Fe_2(CO)_3(\mu\text{-}CO)(CN)_2\{MeSCH_2C(Me)(CH_2S)_2\}]^{2-}$ (**D**; Scheme 1). This species possesses key attributes of the natural sub-site, a 2Fe3S core, a bridging CO, and CN groups ligating each Fe atom. **D** slowly rearranges to the thermodynamically stable product $[Fe_2(CO)_4(CN)_2\{MeSCH_2C(Me)(CH_2S)_2\}]^{2-}$ (**E**), in which the bridging carbonyl ligand has switched to a terminal bound mode with concomitant dissociation of the thioether ligand (Scheme 1).

Kinetic data are consistent with both the initial cyanation of the {2Fe2S} complex $[Fe_2(CO)_6\{CH_2(CH_2S)_2\}]$ and that of the {2Fe3S} complex **A** taking place by an associative mechanism.[11,24] However, the reaction rate for monocyanation of the {2Fe3S} species **A** is about 10000-fold larger than that observed for the {2Fe2S} species.[24] Other major differences are related to the substitution of CO by a second cyanide ligand. In particular, spectroscopic data are consistent with the presence of a μ-CO group in **D**, whereas no long-lived intermediates featuring bridging CO have been characterised along the pathway to $[Fe_2(CO)_4(CN)_2\{CH_2(CH_2S)_2\}]^{2-}$.

Density functional theory (DFT) is a valuable tool to study properties of models of metal-containing enzymes,[25] and theoretical investigations of models related to the Fe-only hydrogenase active site have been recently reported.[26–31] In particular, DFT has been successfully used to study the fluxional properties of {2Fe2S} clusters,[26] to predict structures and redox states of intermediate species formed in the catalytic cycle of the enzyme,[27,28] to explore the structure and reactivity of {2Fe2S} models[29] and to complement experimental data in the characterisation of biomimetic synthetic complexes.[30,31]

Herein we describe a DFT investigation of the mechanism of cyanation of the {2Fe3S} complex **A** that complements kinetic and spectroscopic data obtained for intermediate species in the substitution pathway, including **D**, and provides a deeper insight into the intimate mechanism of cyanation of the dinuclear assembly. Importantly, in silico elucidation of the structural and electronic properties of the intermediate **D** is pertinent to the enzyme sub-site in its CO inhibited form. In a wider context, the study provides an insight into intermediate species and transition states involved in substitution at dinuclear carbonyl species, into the role of bridging CO in such substitution pathways, and clarifies how a neighbouring group with the capability of on/off coordination can influence reactivity.

We first validate the computational method by comparing calculated structures and spectroscopic data with that obtained for the species **A** and **C**, whose structures have been established by X-ray crystallography. We then examine the

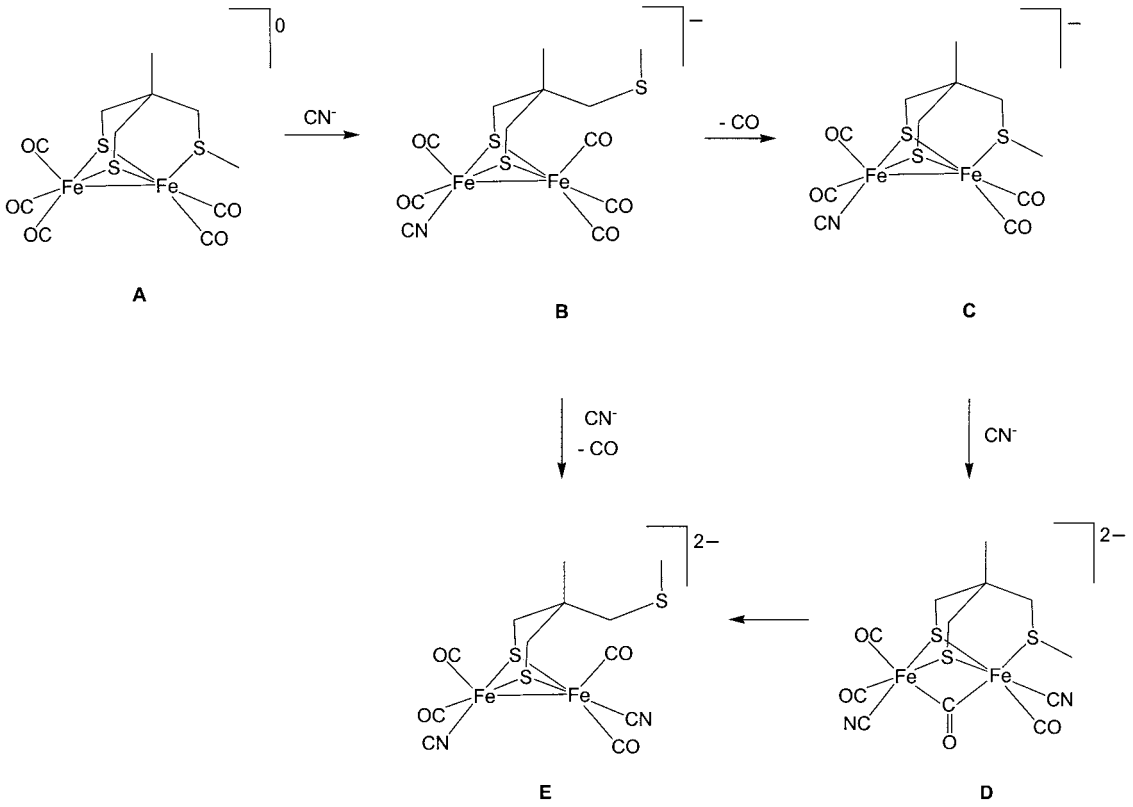

Scheme 1. Summary of the cyanation chemistry of **A**.

first cyanation step and show that, as intimated from the kinetic studies, the DFT results are consistent with the formation of a bridging carbonyl transition state, $[Fe_2(CO)_4(\mu\text{-}CO)(CN)\{MeSCH_2C(Me)(CH_2S)_2\}]^-$. We then go on to show how this can lead to the stable intermediate **B**, and by CO loss to isolable **C**. Penultimately, we examine the second cyanation step defining the transition-state which leads to **D**, which then rearranges to **E**. Finally, we show that the correspondence of calculated and experimental IR data further support the structural assignment of **D**.

Results and Discussion

Three intermediate species along the pathway going from **A** to **E** have been experimentally characterised (**B**, **C** and **D**; see Scheme 1). The structures of **A** and **C** have been determined by X-ray diffraction,[32] whereas the structures of **B**, **D** and **E** have been assigned on the basis of spectroscopic data.[24] Hereafter, experimental complexes are designated by bold upper case letters (**A**, **B**, **C…**) as in Scheme 1 and their *corresponding* computational structures by lower case letters (**a**, **b**, **c**···). Fe1 and Fe2 refer, respectively, to the iron atoms distal and proximal to the R-S-CH_3 arm of the chelating ligand.

Validation of computational results: Initially, with the aim of verifying whether the adopted DFT approach (BP86/TZVP; see Methods) is suitable to describe this class of compounds, we have optimised the structures of the theoretical models **a** and **c** (see Figure 2) and compared them with the corresponding experimental structures **A** and **C** (see Table 1). Computed bond lengths are within ± 0.02 Å of those determined experimentally, with the exception of Fe–S distances involving bridging sulfur atoms, which are systematically overestimated by about 0.04 Å. The adoption of other functionals commonly used to investigate coordination compounds, such as B3LYP,[33] leads to similar or slightly poorer results (data not shown), as previously observed for other Fe–S species.[34] BP86/TZVP predicts that, in the gas phase, the most stable **c** isomer is characterised by axial orientation of the CN group, whereas the equatorial isomer, which is experimentally observed in the solid state,[32] is slightly less stable ($\Delta E = 2.1$ kcal mol^{-1}). The presence of almost isoenergetic cyanide positional isomers, whose relative stability can be affected by crystal packing forces that cannot be taken into account in the calculations, was already noted in investigations of similar species.[9,13] Notably, the inclusion of zero-point vibrational (plus thermal enthalpy), solvation and entropy effects reverse the relative stability of the **c** isomers, leading to the prediction that the equatorial isomer is slightly more stable ($\Delta G = -1.1$ kcal mol^{-1}; Table 2), in agreement with experimental data. Thus the Fe–CN bond length computed for the isomer of **c** in which the CN^- group is equatorial (structure not shown) is in good agreement with experimental values, whereas the corre-

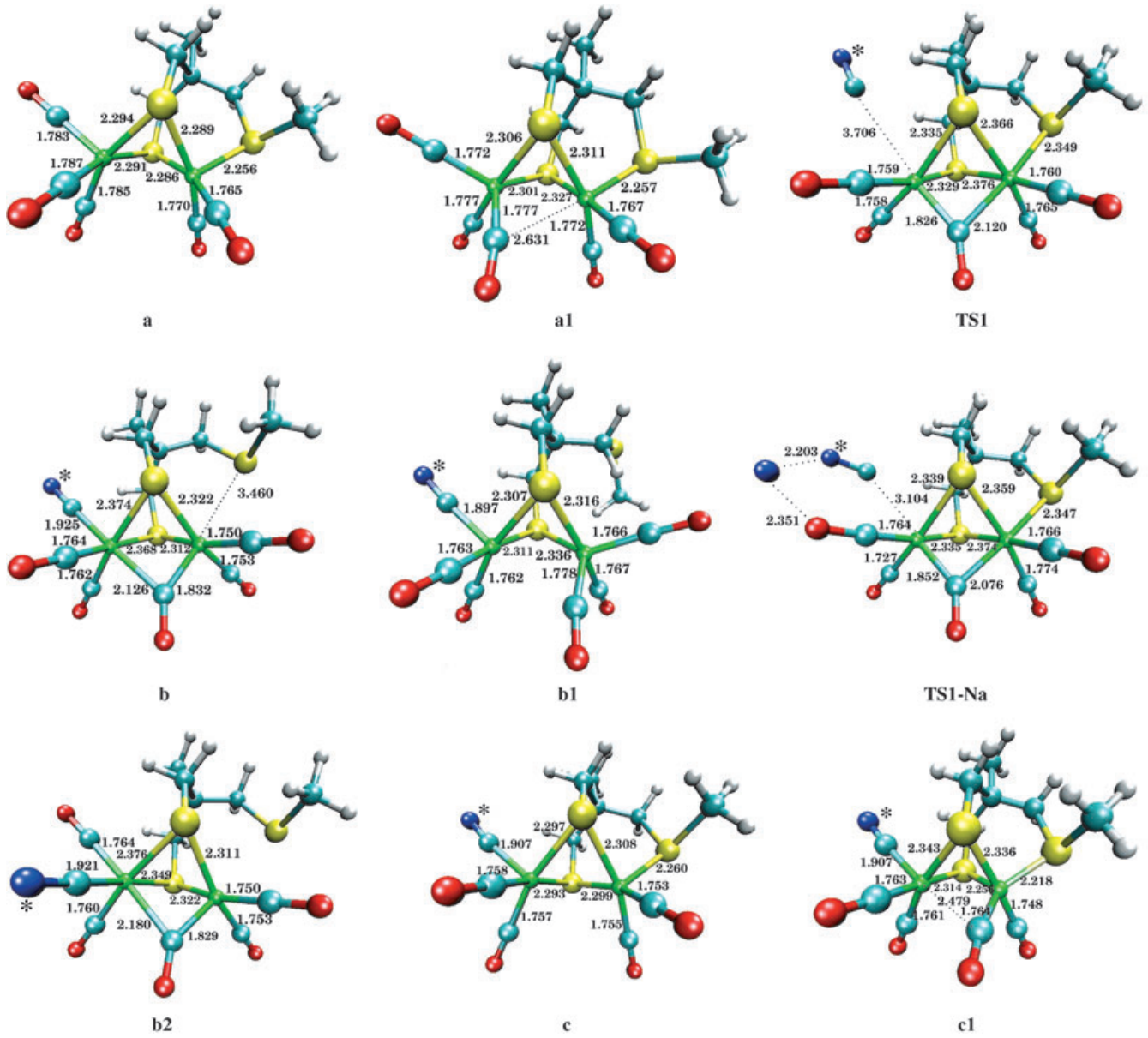

Figure 2. Optimised structures of the investigated $\{Fe_2S_3\}$ complexes. Selected distances are in Å. N atoms of CN ligands are labeled with * to easily distinguish between N and O atoms.

sponding bond length for the axial isomer shows poorer correspondence (Table 1).

The Fe–Fe distances, which are expected to be affected by subtle differences of the electronic properties of the complexes, are well reproduced both in **a** and **c**, the error being less than 0.03 Å. Also the differences between experimental and computed bond angles are very small (lower than 5°; data not shown), confirming that the adopted computational scheme is well suited to investigate the structural properties of this class of compounds.

The comparison of experimental and computed vibrational frequencies of CO and CN groups can help in defining the structural properties of coordination compounds for which the X-ray experimental structure is not known. Therefore, to complete the evaluation of the adopted DFT protocol, we have compared the computed vibrational frequencies of CO and CN groups in **a** and **c** models with the corresponding experimental values. The good agreement between experimental and computational data (Table 3) shows the adequacy of the adopted level of theory also for the reproducibility of the spectroscopic data, and confirms previous observations indicating that harmonic wave numbers from BP86 calculations compare well with experimental data, with the *caveat* that the excellent agreement is in some part due to an error cancellation effect.[35,36]

The first cyanation step: Experimental data support a mechanism in which the monocyanation of **A** proceeds through

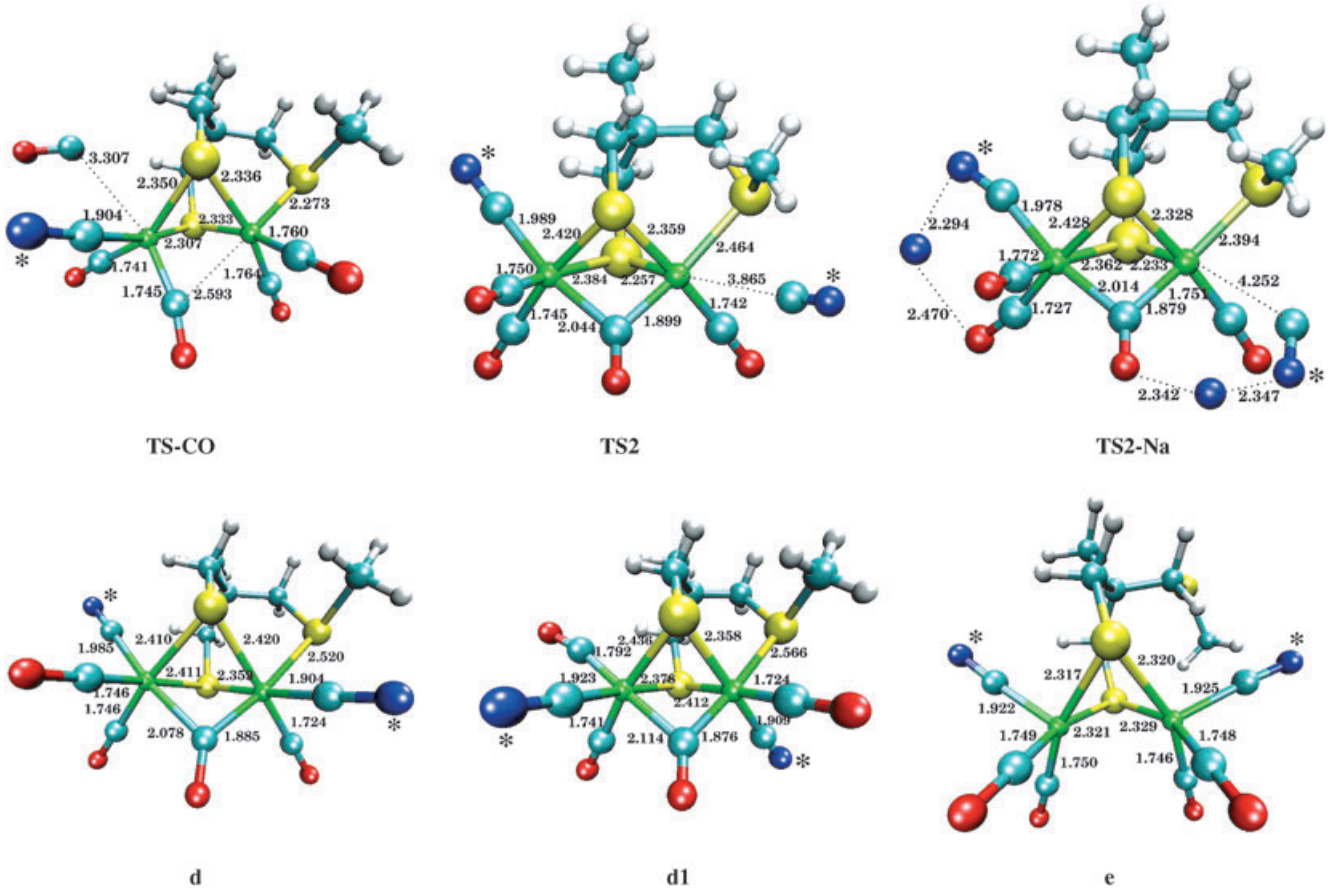

Figure 2 (cont.)

Table 1. Comparison of selected bond lengths (in Å) obtained for experimentally characterised $\{Fe_2S_3\}$ complexes (upper case,[15,24]) and their corresponding computational models (lower case). S_t and S_b stand for terminal and bridging sulfur atoms, respectively.

	a	**A**	**c**	**C**
Fe2–S_t	2.256	2.261	2.260	2.255
Fe2–S_b	2.286	2.251	2.299	2.260
	2.289	2.251	2.308	2.265
Fe2–CO	1.765	1.755	1.753	1.752
	1.770	1.764	1.755	1.761
Fe1–S_b	2.291	2.255	2.293	2.241
	2.294	2.256	2.297	2.249
Fe1–CO/CN	1.783	1.779	1.757	1.761
	1.785	1.795	1.758	1.765
	1.787	1.795	1.907	1.941
			(1.922)[a]	
Fe1–Fe2	2.536	2.516	2.567	2.538

[a] The value in parenthesis refers to the isomer in which the cyanide group occupies an equatorial position, as observed in the X-ray structure of **C**.

Table 2. Energetics for the cyanation of $[Fe_2(CO)_5\{MeSCH_2C(Me)(CH_2S)_2\}]$.[a]

	ΔG	ΔE_{gas}	ΔE_{solv}	$\Delta G - \Delta E_{solv}$
a→**a1**	3.1	4.6	3.7	−0.6
a1 + CN^-→**TS1**	5.8	4.5	2.5	3.3
TS1→**b**	−19.4	−28.5	−17.7	1.7
b→**b1**	−8.2	−8.2	−6.4	−1.8
b1→**b2**	8.3	14.7	7.4	0.9
b2→**TS-CO**	15.5	22.9	17.5	−2.0
TS-CO→**c** + CO	−16.6	−11.4	−8.2	−8.4
c→**c1**	11.9	10.9	11.9	0.0
c1 + CN^-→**TS2**	34.9	47.7	26.2	8.7
TS2→**d**	−38.5	−40.0	−41.6	3.1
d→**e**	−8.2	−16.8	−7.0	−1.2
a + Na^+ + CN^-→**TS1-Na**$^+$	12.5	2.2	7.0	5.5
c + $2Na^+$ + CN^-→**TS2-Na**$^+$	49.5	26.9	45.4	4.1
Fe_2S_2 + CN^-→**TS**	12.6	12.1	10.4	2.2
Fe_2S_2 + Na^+ + CN^-→**TS-Na**	18.4	6.7	13.2	5.2
Fe_2S_2 (+$2Na^+$ + CN^-; second cyanation step)	21.4	11.6	16.3	5.1

[a] ΔE_{gas} = SCF total energy values computed for isolated molecules, ΔE_{solv} = SCF total energy values computed according to the COSMO model for solvation, $\Delta G - \Delta E_{solv}$ = free energy values computed taking into account zero-point vibrational (plus thermal enthalpy) and entropy effects. Energy values in kcal mol^{-1}.

the formation of the intermediate species **B** (Scheme 1). This intermediate is an analogue of the isolable species $[Fe_2(CO)_5(CN)\{CH_2(CH_2S)_2\}]^-$, which has been characterised crystallographically[12] and which shows an IR spectrum essentially identical to that of **B**. The intimate mechanism of the conversion of **A** to **B** has been argued to proceed via a transition state structure in which a CO group bridges the two iron atoms.[24] We have used DFT to further probe this

Table 3. Experimental and computed CO and CN^- frequencies (cm^{-1}) for the Fe^IFe^I di-iron complexes **A**, **B**, **C**, **D** and **E** and their corresponding computational models.

Complex **A**			Complex **B**			Complex **C**			Complex **D**			Complex **E**	
Exp.	**a**	**a1**	Exp.	**b**	**b1**	Exp.	**c**	**c1**	Exp.	**d**	**d1**	Exp.	**e**
1927	1951	1947	1915	1817	1922	1890	1903	1866	1780	1726	1765	1873	1875
	1971	1964	1947	1919	1929	1905	1925	1926	1878	1878	1856	1884	1898
1983[a]	1988	1972	1957	1958	1945	1941	1939	1941	1919	1900	1886	1922	1912
	1991	1998	1976	1969	1971	1981	1981	1993	1957	1952	1934	1963	1955
2048	2044	2035	2031	2009	2008	2085	2095	2108	2075	2075	2081	2076	2071
			2092	2108	2106				2083	2080	2101		2075

[a] Broad.

hypothesis and fully dissect the cyanation reaction. In the following, unless stated differently, energy values are free energy differences, computed by adding to the SCF total energy, solvation effects, zero-point vibrational (plus thermal enthalpy) contribution, as well as entropy effects (see Methods). The detailed mechanism and energetics for the cyanation of **a** are summarised in Scheme 2 and 3, and in Table 2.

The $Fe(CO)_3$ group at Fe1 in **A** would be expected to rotate relatively easily, as observed at *both* Fe atoms in $[Fe_2\{CH_2(CH_2S)_2\}(CO)_6]$,[30] whereas at Fe2 the coordinated R-S-CH_3 arm locks the configuration thereby restricting rotation. Thus geometry optimisations from $[Fe_2(CO)_5\{MeSCH_2C(Me)(CH_2S)_2\}]$ show that, in structures where the $Fe(CO)_3$ group is slightly rotated with respect to **a**, an energy-minimum structure is obtained (**a1**, see Figure 2) that resembles the computed transition state arising from the rotation of an $Fe(CO)_3$ group in $[Fe_2\{CH_2(CH_2S)_2\}(CO)_6]$.[30] In **a1**, the coordination environment of Fe1 is better described as a trigonal bipyramid, with one CO and one S ligand in axial position, and with one equatorial CO group approaching the proximal Fe2 centre. Importantly, the rotation of the $Fe(CO)_3$ group leads to the incipient formation of a vacant coordination position *trans* to the semi-bridging CO group.

The observation that **a1** is a stable intermediate species, whereas the corresponding structure for the $[Fe_2\{CH_2(CH_2S)_2\}(CO)_6]$ computational model corresponds to a saddle point on the potential energy surface (i.e. a transition state structure), underscores the role of the R-S-CH_3 ligand in stabilising bridging-CO species. In fact, the conversion **a**→**a1** is endoergonic by only 3.1 kcal mol^{-1}. The comparison of atomic charges for **a** and **a1** reveals that the movement of a CO group from terminal to semi-bridging position is accompanied by an increase in the electrophilicity of the distal Fe1 atom (not shown).

The computed structure of the transition state (**TS1**) corresponding to the attack of CN^- on **a1** is shown in Figure 2. In **TS1** the distal Fe1 atom has a distorted octahedral geometry, in which one of the ligands is the approaching CN^- group. A CO group bridges the iron atoms in a quasi-symmetric fashion and the bond between the proximal Fe2 centre and the terminal sulfur ligand is elongated (2.35 Å) with respect to **a** and **a1** (2.26 Å), indicating that the thioether group functions as a good leaving group. The computed potential free energy barrier for the cyanation of **a1** to give **TS1** is 5.8 kcal mol^{-1}.

In principle, the cyanation of **a** could proceed *via* other reaction pathways (Scheme 4). In the transition state structure in which the distal Fe1 centre could still be pseudo-octahedral,

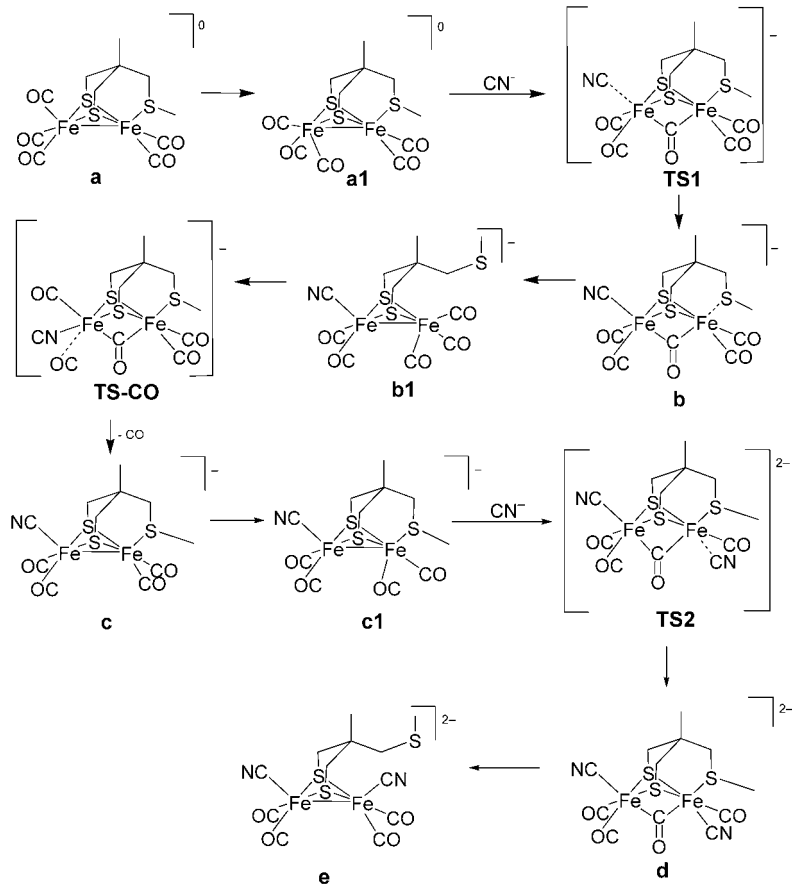

Scheme 2. Computed reaction path for the cyanation of **a**.

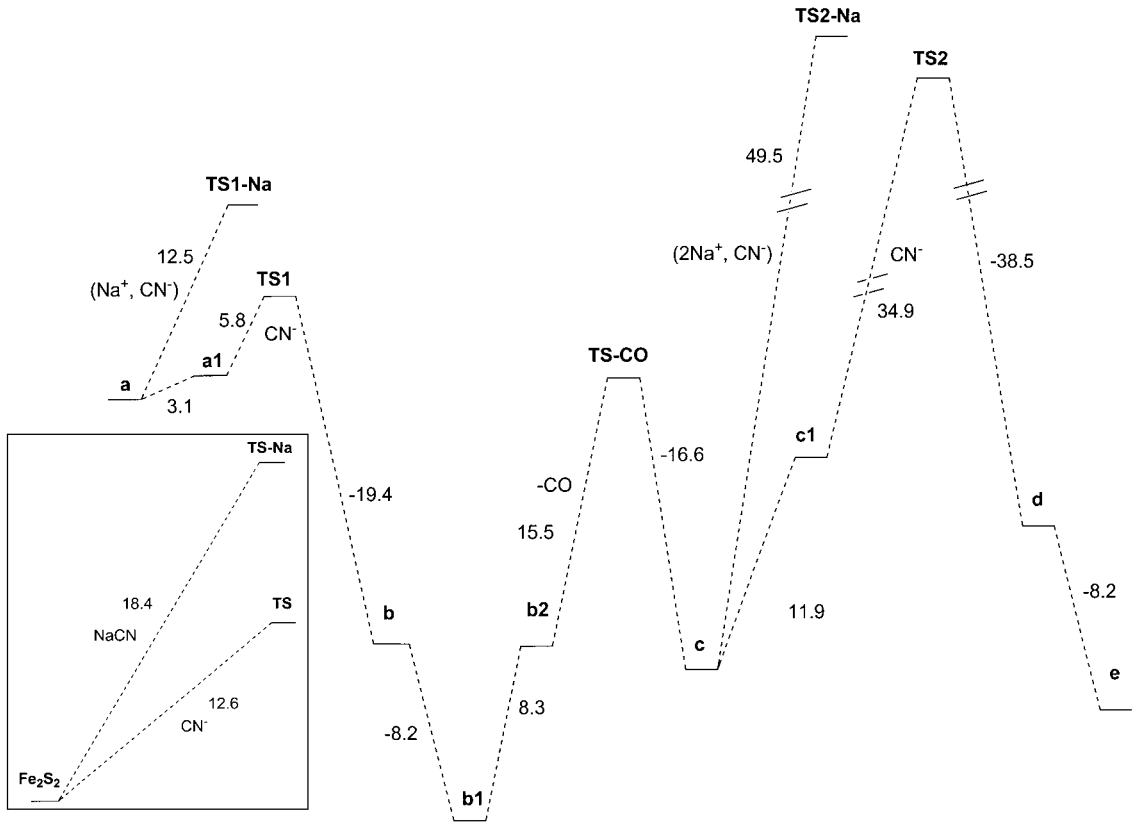

Scheme 3. The energetics (kcal mol^{-1}) for the cyanation of **a**. The energy barriers for the first cyanation of the {2Fe2S} complex [(μ-pdt)$Fe_2(CO)_6$] are reported in the inset.

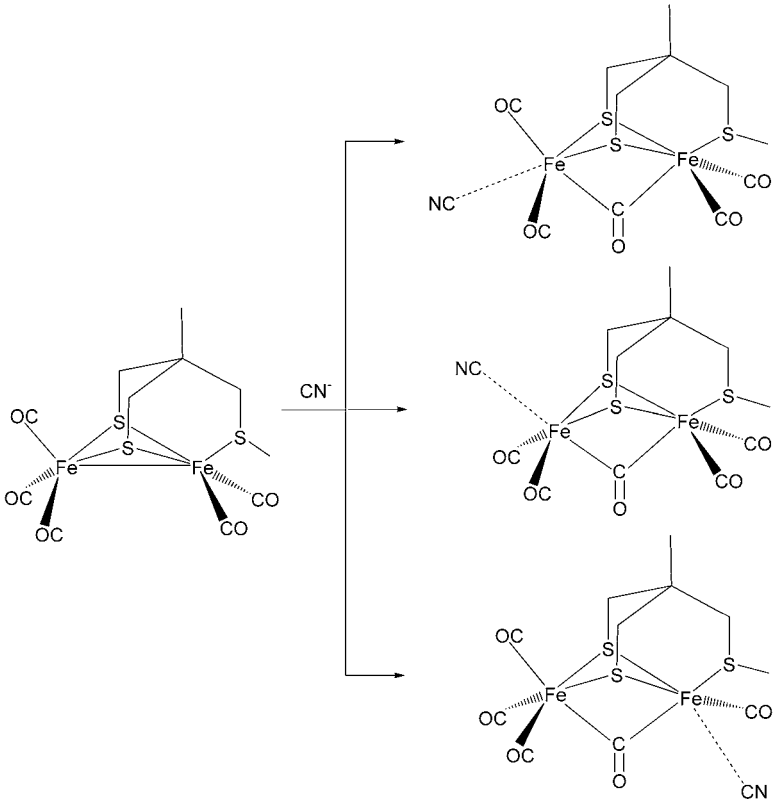

Scheme 4. Possible reaction coordinates for the first cyanation of **a**.

the CN^- group could attack *trans* to one of the sulfur atoms bridging the two metal centres (Scheme 3). However, the computed energy barrier for this reaction coordinate is very large (>25.0 kcal mol^{-1}), indicating that this reaction channel is kinetically unfavourable. The large energy barrier can be mainly attributed to the presence of a strong σ-donor *trans* to the approaching CN^- group. To study the factors affecting the regiospecificity observed in the cyanation of **a**, we have investigated also a reaction path where the incoming CN^- group approaches the Fe2 ion. The hindered ligand rotation at Fe2 imposed by coordination of the thioether ligand restricts approach of CN^- to a reaction coordinate *trans* to one of the bridging S atoms (Scheme 4). The corresponding free energy

barrier for this reaction channel is 35.2 kcal mol^{-1} and is thus also unfavourable with respect to that going through **TS1**.

To assess possible effects due to the different charge of the reactant (**a1**; charge = 0) and the transition state (**TS1**; charge = −1), we have computed the transition state structure (**TS1-Na**) obtained considering NaCN as the cyaniding species, as done in an earlier investigation addressing the cyanation of the {2Fe2S} species $[Fe_2(CO)_6\{CH_2(CH_2S)_2\}]$.[30] We find that the structures of **TS1** and **TS1-Na** are very similar, differing markedly only in the distance between the attacking CN^- group and Fe1 (Figure 2). Optimisation of reagents, that is, the van der Waals adduct between **a1** and NaCN, led to a species resembling **a**, in which the semi-bridging CO group has moved to a terminal position (not shown), an observation which indicates that ion-pairing can modulate to some extent the coordination geometry of Fe1. However, the computed potential free energy barrier for the reaction **a** + NaCN → **TS1-Na** is still small (decreased to 12.5 kcal mol^{-1}; Scheme 3). Most importantly, the other conceivable reaction paths (Scheme 4) are characterised by very large energy barriers (> 35 kcal mol^{-1}).

As stated above, the experimental reaction rate for monocyanation of the {2Fe3S} species **A** is some 10^4 times faster than that observed for the {2Fe2S} species $[Fe_2(CO)_6\{CH_2(CH_2S)_2\}]$.[24] To probe this difference we have also computed the transition state along the cyanation pathway leading to the {2Fe2S} species $[Fe_2(CO)_5(CN)\{CH_2(CH_2S)_2\}]$. This latter reaction path was investigated in an earlier study by Hall et al.,[30] who found a transition state structure characterised by a μ-CO group and a corresponding activation energy of 13.60 kcal mol^{-1}. Their investigation was carried out using the B3LYP functional and maintaining a neutral model system by addition of Na^+ counter-ions. The B3LYP functional generally predicts slightly larger barriers than BP86,[37] making the direct comparison of the computational data for the two systems problematic. We have therefore re-investigated the cyanation of $[Fe_2(CO)_6\{CH_2(CH_2S)_2\}]$ at the BP86/TZVP level of theory, including also solvation effects, to allow a fair comparison with results obtained for the {2Fe3S} system. It should be noted that both iron centres are equivalent in the $[Fe_2(CO)_6\{CH_2(CH_2S)_2\}]$ complex, at least within the time scale of the ring flip, whereas only the distal Fe1 centre undergoes attack in **A**. However, this statistical effect is not expected to influence significantly DFT results. We find that the potential free energy barriers computed for the cyanation of $[Fe_2(CO)_6\{CH_2(CH_2S)_2\}]$, with CN^- or NaCN as reactants, are 12.6 and 18.4 kcal mol^{-1}, respectively. Hence, the presence of the thioether group decreases the energy barriers for the cyanation reaction by 6.8 kcal mol^{-1} (CN^-) and 5.9 kcal mol^{-1} (NaCN), in full agreement with experimental observations. This effect is consistent with the thioether ligand both stabilising the incipient bridging CO vis a vis a terminal CO at Fe2, in agreement with the proposal that the $Fe(CO)_3$ rotational barrier is an important contributor to the overall activation energy for CN^- attack,[30] and functioning as a good leaving group in the concerted associative process at the binuclear assembly.

The optimised structure of **b**, which is more stable than **TS1** by about 19.4 kcal mol^{-1} and is the product of CN^- attack on **a1**, retains a μ-CO group, whereas the interaction between Fe2 and the thioether sulfur atom is very weak (Figure 2). Notably, the sampling of the potential energy hypersurface led to the identification of a more stable isomer of the product of monocyanation (**b1**; see Figure 2). In **b1**, the thioether sulfur atom is not coordinated to Fe2 and the bridging CO group observed in **b** moves to a semi-bridging position in **b1**, with the geometry about the proximal Fe centre better described as a distorted trigonal bipyramid. The comparison of relative energies reveals that **b** is less stable than **b1** by 8.2 kcal mol^{-1}, in agreement with the observation that a species corresponding to **b** is not detected experimentally as the primary product of monocyanation. Notably, the more stable metal—metal-bonded isomer **b1** closely corresponds to the structure assigned to the intermediate species **B** from spectroscopic data (see below).

To complete the characterisation of the monocyanide species we have computed the structure of (chiral) isomers that differ from **b1** in having CN^- in (either) equatorial position. In these species, the semi-bridging CO group moves to a terminal position and the iron atoms have a regular square-pyramidal coordination environment (not shown). This observation highlights again the stabilising role of a donor ligand in a *trans* position to the bridging CO. The **b1** isomers characterised by an equatorial CN^- are less stable than the corresponding axial isomer by 3–5 kcal mol^{-1}.

The reversible CO loss/thioether re-binding step: Experimental data show that the complex $[Fe_2(CN)(CO)_5\{MeSCH_2C(Me)(CH_2S)_2\}]^-$ (**B**) reversibly loses CO to form the isolable {2Fe3S} species **C**, in which the thioether group is coordinated to the proximal Fe2 atom as in the parent complex **A** (Scheme 1). The regiospecificity of CO rebinding to **C** has been investigated by FTIR spectroscopy using $^{13}C^{18}O$ and results are consistent with the labelled CO attacking the cyanide-ligated Fe1 atom, concerted migration of an unlabelled CO ligand and concomitant dissociation of thioether from Fe2.[24]

To gain an insight into the **B** → **C** + CO step, we have optimised the structure of the transition state related to CO loss (**TS-CO**), taking as the reactant a **b** isomer in which the CN^- group is coordinated to Fe1 in an equatorial position (**b2**; Figure 2).[38] In **b2**, which is less stable than **b** by 8.3 kcal mol^{-1}, a CO group is *trans* to the μ-CO and can act as a leaving group according to a mechanism that implies transfer of CO from Fe2 to Fe1, concerted cleavage of the Fe1−CO bond, and coordination of the thioether ligand to Fe2. In fact, in **TS-CO**, an Fe1 bound CO group moves to a semi-bridging position, the Fe1-(μ-CO) distance becomes very short (1.75 Å) and the bond length between Fe1 and the CO group *trans* to the μ-CO increases to 3.31 Å (Figure 2).

The computed structural features, together with the observation that no other transition state structures were found along the pathway from **b2** to **c**, indicate that the thioether re-binding to Fe2 is accompanied by CO loss from the terminal Fe1 centre. **TS-CO** is less stable than **b2** by 15.5 kcal mol^{-1}, in good agreement with the relatively slow reaction rate for the **B**→**C** + CO conversion.[24]

The second cyanation step: Cyanation of the complex $[Fe_2(CN)(CO)_4\{MeSCH_2C(Me)(CH_2S)_2\}]^-$ (**B**) can take place following two different reaction paths (Scheme 1). In the presence of a large excess of CN^-, **B** is directly converted to **E** (high-cyanide pathway), whereas if the CN^- concentration is lower, **B** initially loses one CO group forming the species **C** (see above). Subsequently, **C** reacts with CN^- forming the μ-CO intermediate **D**, which eventually converts to the thermodynamically more stable form **E** (low-cyanide pathway). The high cyanide pathway is kinetically disfavoured with respect to the low-cyanide pathway. In addition, cyanation of the {2Fe3S} species **B** is slower than for the corresponding {2Fe2S} complex $[Fe_2(CO)_5(CN)\{CH_2(CH_2S)_2\}]^-$.

With the aim of characterising intermediate and transition state species relevant to the second cyanation step, we have initially sampled the potential energy surface searching for possible other isomers of **c**. As observed for **a**, we located an isomer that is characterised by a distorted trigonal-bipyramidal geometry of the proximal Fe2 centre, (**c1**; Figure 2). In **c1**, which is less stable than **c** by 11.9 kcal mol^{-1} (Scheme 3), the equatorial CO group is semi-bridged between the two metal ions and an incipient vacant coordination site appears on the Fe2 centre. It is worth noting that the vacant coordination sites in **c1** and **a1** are different, being *trans* to a μ-S atom and to a μ-CO group, respectively (Figure 2). In contrast to **a** and **a1**, the partial atomic charges computed for the Fe2 atom are not dissimilar in **c** and **c1** (data not shown)

The computed structure of the transition state corresponding to the attack of CN^- on **c1** (**TS2**) is shown in Figure 2. In **TS2**, which is 34.9 kcal mol^{-1} higher in energy than reactants (**c1** + CN^-), the proximal Fe2 atom has a distorted octahedral geometry where one of the ligands is the approaching CN^- group. A CO group bridges the iron atoms in a quasi-symmetric fashion and the bond between Fe2 and the terminal sulfur ligand is elongated (2.46 Å) with respect to **c** and **c1**. To obtain unbiased results, we have also computed the transition state for the electro-neutral system that includes two Na^+ ions, (**TS2-Na**). The structures of **TS2** and **TS2-Na** are very similar, differing significantly only in the distance between the attacking CN^- group and the proximal iron centre (Figure 2). As observed for the first cyanation step, optimisation of the van der Waals reactant complex (**c1** + 2Na^+ + CN^-) leads to an adduct in which the bimetallic cluster rearranges to a structure resembling **c**. The free energy barrier associated with **TS2-Na** is 49.5 kcal mol^{-1} (Table 2 and Scheme 3).

Again for comparison with the corresponding {2Fe2S} system, we have computed the transition state for the attack of NaCN on $[Fe_2(CO)_5(CN)\{CH_2(CH_2S)_2\}]Na$, obtaining a free energy barrier of 21.4 kcal mol^{-1}. Notably, the free energy barrier is slightly larger than that for the first cyanation step, in disagreement with experimental data for this system[8–10] as also found by Hall and co-workers.[30] They have argued that the error is due to the presence of Na^+ ions, which artificially increase the rotation barrier for the FeL_3 group. This observation suggests some care in the discussion of small energy differences in computed activation barriers. However, the energy difference between the free energy barrier for the second cyanation step of the {2Fe2S} system (21.4 kcal mol^{-1}) and the corresponding value computed for the {2Fe3S} system (49.5 kcal mol^{-1}) is very large and in good agreement with the experimental observation that $\{Fe_2S_2\}$ systems react faster.[24]

The difference between {2Fe2S} and {2Fe3S} systems in the second cyanation step reflects deactivation of the Fe2 atom towards nucleophilic attack due to coordination of the electron-donating thioether group to Fe2. In the van der Waals reactant complex (**c1** + 2Na^+ + CN^-) the Fe2 atom is only slightly less electrophilic than the corresponding iron atom in $[Fe_2(CO)_5(CN)\{CH_2(CH_2S)_2\}]Na$ (data not shown), suggesting that the electron-donor character of the thioether group is not the only cause for the difference in reactivity between **c** and $[Fe_2(CO)_5(CN)\{CH_2(CH_2S)_2\}]^-$. Other key factors affecting the reactivity of **c** are the hindered rotation of ligands at the Fe2 group due to the 'locking' coordination of the thioether ligand, documented by the large energy difference between **c** and **c1** (compared to **a** and **a1**; Table 2), and the different reaction coordinate of the approaching CN^- group, which attacks *trans* to an electron-withdrawing CO group and to an electron donor S ligand in the {2Fe2S} and {2Fe3S} complexes, respectively.

The optimised structure of **d**, which is the product of the second cyanation, is more stable than **TS2** by 38.5 kcal mol^{-1} (Table 2 and Scheme 3). In **d**, one CO group bridges in a quasi-symmetric fashion the two iron atoms and the distance between the proximal Fe2 centre and the thioether ligand is relatively long (2.520 Å), suggesting that this bond can be easily cleaved. However, it should be noted that the corresponding distance observed in **b** is significantly longer (3.460 Å), indicating that the conversion of **d** to **e**, in which both iron centres are five-coordinate (Figure 2), implies the cleavage of *both* the Fe1–μCO and Fe2–S bonds, whereas only the cleavage of the Fe1–μCO bond is necessary to convert **b** to **b1** (see above). The experimental observation that the attack of CN^- on **C** gives the μ-CO intermediate **D**, whereas attack on **B** does not give a spectroscopically detectable CO-bridged species can be rationalised as follows. Comparison of **b** and **d** might suggest that the partial charge on Fe2 is more negative in **d** than in **b**, due to the coordination of the donating R-S-CH_3 and the anionic CN^- donor groups in the former. However, we find that the partial atomic charge on Fe2 in **d** and **b** are very similar, (−0.75 and −0.76, respectively), whereas the electron density on

the CO groups coordinated to Fe2 increases significantly moving from **b** to **d**. Thus, the electron-accepting terminal and bridging CO groups provide a sink for the extra charge brought in by the cyanide and thioether coordination at Fe2. We conclude that in **b** the strongly electron-demanding ketonic μ-CO group is destabilised by the presence of the other π-acceptor ligands, triggering metal–metal-bond formation and concomitant cleavage of the bond between Fe2 and the thioether ligand necessary to maintain an 18-electron configuration at the Fe2 centre. On the other hand, substitution of a CO group with a stronger donor such as CN^- results in a sufficiently electron-rich Fe2 atom in **d** to trigger the cleavage of the metal-metal bond, disperse electron density by efficient donation into the μ-CO group, and allow coordination of the thioether ligand to Fe2, satisfying again the 18-electron rule.

Isomeric forms of **d1** may exist which differ in the orientation of the cyanide groups. We find that an isomer in which both cyanide ligands are *trans* to the bridging thiolate groups and have *anti*-configuration (**d1**; Figure 2) is $< 2\ kcal\,mol^{-1}$ less stable than **d** (i.e. differing by less than the accuracy of the method) but, as expected, with less charge transmitted to the bridging CO the IR frequency of this group is raised (see discussion of **d1** and **D** below).

The structure **e** is more stable than **d** by about $8.2\ kcal\,mol^{-1}$, in close accord with the experimental observation that **D** rearranges to the thermodynamically more stable isomer **E**.

Spectroscopic properties and structure assignment: The structures of the complexes **A** and **C** have been established by X-ray diffraction, whereas structural assignments for all the other detected intermediate species have been based on comparative IR data with structurally characterised analogues (**B**, **E**) or by inference **D**.[24] Therefore, in light of the good agreement between experimental and computed vibrational frequencies observed for **A** and **C** (see above), and with the aim of evaluating the structural assignment for **B**, **D** and **E**, we have extended the comparison to the other {2Fe3S} species. The vibrational frequencies for CO and CN groups computed for the {2Fe3S} models investigated in this work are collected and compared to the corresponding experimental values in Table 3.

The computed vibrational frequencies for **a1** are not markedly different from those computed for the more stable isomer **a**. In particular, the frequency associated with the stretching of the semi-bridged CO decreases only by a few cm^{-1} moving from **a** to **a1**, consistent with the weak interaction between the CO group and Fe2. The corresponding difference between **c** and **c1** is larger, due to the stronger Fe1–CO interaction. However, the experimental values are closer to those computed for **c**, in agreement with the computed relative stability for these two isomers.

Comparison of computed vibrational frequencies for **b** and **b1** with the corresponding experimental values reveals that **b1** corresponds to the structure observed in solution, in agreement with the computed relative energies of these isomers and with the assignment made on the ground of experimental data.[24] Very good agreement among computed and experimental data is observed comparing the values for **e** and **E**, also in this case confirming the structural assignment made on the basis of IR data. The same good agreement holds true also for the terminal CO frequencies for **D** and **d** species, but the value for the bridging CO is significantly different. The isomer **d1**, which differs from **d** in having equatorial cyanide ligands in an *anti*-configuration, is only very marginally less stable than **d**, as discussed above. Importantly, **d1** is characterised by *all* stretching frequencies in very good agreement with the experimental data,[24] as shown by the plot in Figure 3 and the data in Table 3. We therefore conclude that **D** with equatorial cyanide at Fe1 is most likely the dominant isomer in solution.

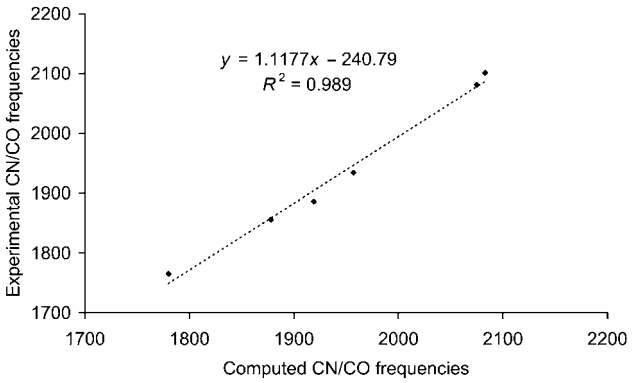

Figure 3. Correlation of the calculated and observed CN^- and CO frequencies (cm^{-1}) for **D** and **d1**.

Conclusion

We have used DFT to described the intimate mechanism of the pathway of substitution of an {2Fe3S}-carbonyl species by CN^- in terms of structures, energetics and IR spectroscopy. This has:

1) provided an explanation for the regioselectivity and the enhanced rate of monocyanation of {2Fe3S} vis a vis {2Fe2S} carbonyls in terms of a pathway allowing on/off coordination of a thioether ligand bound at the *neighbouring* iron atom,
2) shown that the difference between {2Fe2S} and {2Fe3S} systems in the second cyanation step not only reflects deactivation of the Fe2 atom, due to coordination of the electron-donating thioether group, but is due also to the hindered rotation at Fe2 group and the different reaction coordinate of the approaching CN^- group in {2Fe2S} and {2Fe3S} systems,
3) shown that an incipient carbonyl group bridging the two iron atoms is an important feature of the transition states also in {2Fe3S} systems,
4) provided a computational structure of a detectable intermediate (**d1**) which has key features of the CO inhibited form of the di-iron sub-site of all-iron hydrogenase,

5) shown that computed IR data for this intermediate (**d1**) are in excellent agreement with experimental data for **D** as are data for the X-ray characterised structures (**a**, **c**). This provides a high level of confidence in the computed structure of **D**.

Methods

DFT structure optimisations were carried out by using the BP86 functional[39,40] and an all-electron valence triple-ζ basis set with polarisation functions on all atoms (TZVP).[41] Calculations have been carried out using the Turbomole suite of programs[42] in connection with the resolution of the identity technique.[43,44]

The optimisation of the transition state structures has been carried out according to a procedure based on a pseudo Newton–Raphson method. Initially, geometry optimisation of a guessed transition state structure is carried out constraining the distance corresponding to the reaction coordinate, namely the distance between the attacking cyanide (C atom) and either Fe1 during the first cyanation reaction or Fe2 during the second one. Vibrational analysis at BP86/TZVP level of the constrained minimum energy structures is then carried out and, if one negative eigenmode corresponding to the reaction coordinate is found, the curvature determined at such point is used as the starting point in the transition state search. The location of the transition state structure is determined by using an eigenvector-following search: the eigenvectors in the hessian are sorted in ascending order, the first one being that associated to the negative eigenvalue. After the first step, however, the search is performed by choosing the critical eigenvector with a maximum overlap criterion, which is based on the dot product with the eigenvector followed at the previous step. The exact (analytical) hessian matrix has been finally calculated to carry out the vibrational analysis of the stationary point.

The potential energy barriers have been computed as the difference between the energy of the transition state and the energy of the bimetallic cluster with inclusion of CN^- or NaCN nearby, as optimised together, in conformity with previous investigations.[30] The charge distributions of the complexes were analysed by the Roby–Davidson method.[45–48]

The optimised structures of the complexes reported in the present study correspond always to low spin states, as expected considering the characteristics of the ligands forming the coordination environment of the metal atoms and in agreement with available experimental data.

Derivation of free energy (G) values from the electronic SCF energy has been carried out considering three contributions to the total partition function (Q), namely $q_{\text{translational}}$, $q_{\text{rotational}}$, $q_{\text{vibrational}}$, under the assumption that Q may be written as the product of such terms.[49] To evaluate entalpy and entropy contributions, the value for temperature, pressure and scaling factor for the SCF wavenumbers have been set to 298.15 K, 1 atm and 0.9, respectively. Rotations have been treated classically and vibrational modes described according to the harmonic approximation.

The effect of the solvent (acetonitrile; $\varepsilon = 36.64$) has been evaluated with the continuous model approach COSMO.[50]

The relative energies discussed in the manuscript are Gibbs free energies where the contributions described above are added.

Acknowledgement

M. R. and C. J. P. thank the BBSRC and the John Innes Foundation for supporting this work.

[1] Y. Nicolet, C. Piras, P. LeGrand, C. E. Hatchikian, J. C. Fontecilla-Camps, *Structure* **1997**, *7*, 13–23.
[2] J. W. Peters, W. N. Lanzilotta, B. J. Lemon, L. C. Seefeldt, *Science* **1998**, *282*, 1853–1858.
[3] A. J. Pierik, M. Hulstein, W. R. Hagen, S. P. J. Albracht, *Eur. J. Biochem.* **1998**, *258*, 572–578; A. L. De Lacey, C. Stadler, C. Cavazza, E. C : Hatchikian, V. M. Fernandez, *J. Am. Chem. Soc.* **2000**, *122*, 11232–11233; Y. Nicolet, A. L. De Lacey, X. Vernede, V. M. Fernandez, E. C. Hatchikian, J. C. Fontecilla-Camps, *J. Am. Chem. Soc.* **2001**, *123*, 1596–1601.
[4] D. J. Evans, C. J. Pickett, *Chem. Soc. Rev.* **2003**, *32*, 268–275.
[5] Z. J. Chen, B. J. Lemon, S. Huang, D. J. Swartz, J. W. Peters, K. A. Bagley, *Biochemistry* **2002**, *41*, 2036–2043.
[6] C. V. Popescu, E. Munck, *J. Am. Chem. Soc.* **1999**, *121*, 7877–7884.
[7] A. S. Pereira, P. Tavares, I. Moura, J. J. G. Moura, B. H. Huynh, *J. Am. Chem. Soc.* **2001**, *123*, 2771–2782.
[8] E. J. Lion, I. P. Georgakaki, J. H. Reibenspies, M. Y. Darensbourg, *Angew. Chem.* **1999**, *111*, 3373–3376; *Angew. Chem. Int. Ed.* **1999**, *38*, 3178–3180.
[9] M. Schmidt, S. M. Contakes, T. B. Rauchfuss, *J. Am. Chem. Soc.* **1999**, *121*, 9736–9737.
[10] A. Le Cloirec, S: P. Best, S. Borg, S. C. Davies, D. J. Evans, D. L. Hughes, C. J. Pickett, *Chem. Commun.* **1999**, 2285–2286.
[11] E. J. Lion, I. P. Georgakaki, J. H. Reibenspies, M. Y. Darensbourg, *J. Am. Chem. Soc.* **2001**, *123*, 3268–3278.
[12] F. Gloaguen, J. D. Lawrence, M. Schmidt, S. R. Wilson, T. B. Rauchfuss, *J. Am. Chem. Soc.* **2001**, *123*, 12518–12527.
[13] J. D: Lawrence, H. Li, T. B. Rauchfuss, M. Benard, M.-M. Rohmer, *Angew. Chem.* **2001**, *113*, 1818–1821; *Angew. Chem. Int. Ed.* **2001**, *40*, 1768–1771.
[14] H. X. Li, T. B. Rauchfuss, *J. Am. Chem. Soc.* **2002**, *124*, 726–727.
[15] M. Razavet, S. C: Davies, D. L. Hughes, C. J. Pickett, *Chem. Commun.* **2001**, 847–848.
[16] Z. X. Cao, M. B. Hall, *J. Am. Chem. Soc.* **2001**, *123*, 3734–3742.
[17] H. J. Fan, M. B. Hall, *J. Am. Chem. Soc.* **2001**, *123*, 3828–3829.
[18] M. Bruschi, P. Fantucci, L. De Gioia, *Inorg. Chem.* **2002**, *41*, 1421–1429.
[19] M. Bruschi, P. Fantucci, L. De Gioia, *Inorg. Chem.* **2003**, *42*, 4773–4781.
[20] Z. P. Liu, P. Hu, *J. Am. Chem. Soc.* **2002**, *124*, 5175–5182.
[21] T. Zhou, Y. Mo, A. Liu, Z. Zhou, K. R. Tsai, *Inorg. Chem.* **2004**, *43*, 923–930.
[22] H. Reihlen, A. Gruhl, G. Hessling, *Liebigs Ann. Chem.* **1929**, *472*, 268–275.
[23] D. Seyferth, G. B. Womack, C. M. Archer, J. C. Dewan, *Organometallics* **1989**, *8*, 430–442.
[24] S. J. George, Z. Cui, M. Razavet, C. J. Pickett, *Chem. Eur. J.* **2002**, *8*, 4037–4046.
[25] S. Niu, M. B. Hall, *Chem. Rev.* **2000**, *100*, 353–406; P. E. M. Siegbahn, M. R. A. Blomberg, *Chem. Rev.* **2000**, *100*, 421–438; T. Lovell, F. Himo, W.-G. Han, L. Noodleman, *Coord. Chem. Rev.*

2003, *238–239*, 211–232; R. A. Friesner, M.-H. Baik, B. F. Gherman, V. Guallar, M. Wirstam, R. B. Murphy, S. J. Lippard, *Coord. Chem. Rev.* **2003**, *238–239*, 267–280.
[26] I. Dance, *Chem. Commun.* **1999**, 1655.
[27] S. Niu, M. B. Hall, *Inorg. Chem.* **2001**, *40*, 6201–6203; H.-J. Fan, M. B. Hall, *J. Am. Chem. Soc.* **2001**, *123*, 3828–3829.
[28] Z.-P. Liu, P. Hu, *J. Am. Chem. Soc.* **2002**, *124*, 5175–5182.
[29] M. Bruschi, P. Fantucci, L. De Gioia, *Inorg. Chem.* **2002**, *41*, 1421–1429; M. Bruschi, P. Fantucci, L. De Gioia, *Inorg. Chem.* **2003**, *42*, 4773–4781; M. Bruschi, P. Fantucci, L. De Gioia, *Inorg. Chem.* **2004**, *43*, 3733–3741.
[30] I. P. Georgakaki, L. M. Thomson, E. J. Lyon, M. B. Hall, M. Y. Darensbourg, *Coord. Chem. Rev.* **2003**, *238–239*, 255–266.
[31] See ref. [13] and F. Gloaguen, J. D. Lawrence, T. B. Rauchfuss, M. Benard, M. M. Rohmer, *Inorg. Chem.* **2002**, *41*, 6573–6582.
[32] M. Razavet, S. C. Davies, D. L. Hughes, J. E. Barclay, D. J. Evans, S. A. Fairhurst, X. Liu, C. J. Pickett, *Dalton Trans.* **2003**, 586–595.
[33] A. D. Becke, *Phys. Rev. A* **1988**, *38*, 3098–3104; A. D. Becke, *J. Chem. Phys.* **1992**, *96*, 2155–2160; A. D. Becke, *J. Chem. Phys.* **1993**, *98*, 5648–5652; P. J. Stevens, F. J. Devlin, C. F. Chablowski, M. J. Frisch, *J. Phys. Chem.* **1994**, *98*, 11623–11627.
[34] M. Reiher, *Inorg. Chem.* **2002**, *41*, 6928–6935; O. Salomon, M. Reiher, B. A. Hess, *J. Chem. Phys.* **2002**, *117*, 4729–4737.
[35] J. Neugebauer, M. Reiher, C. Kind, B. A. Hess, *J. Comput. Chem.* **2002**, *23*, 895–910.
[36] J. Neugebauer, B. A. Hess, *J. Chem. Phys.* **2003**, *118*, 7215–7225.
[37] W. Koch, M. Holthausen, *A Chemist's Guide to Density Functional Theory*, 2nd Ed., Wiley-VCH, **2002**, pp. 242–244.
[38] The corresponding transition state obtained by considering the axial cyanide **b1** isomer is **TS1** viz. loss of CN rather than CO.
[39] A. D. Becke, *Phys. Rev. A* **1988**, *38*, 3098–3100.
[40] J. P. Perdew, *Phys. Rev. B* **1986**, *33*, 8822–8824.
[41] A. Schafer, C. Huber, R. Ahlrichs, *J. Chem. Phys.* **1994**, *100*, 5829–5835.
[42] R. Ahlrichs, M. Bar, M. Haser, C. Horn, C. Kolmel, *Chem. Phys. Lett.* **1989**, *162*, 165–169.
[43] K. Eichkorn, O. Treutler, H. Öhm, M. Haser, R. Ahlrichs, *Chem. Phys. Lett.* **1995**, *240*, 283–289.
[44] K. Eichkorn, F. Weigend, O. Treutler, R. Ahlrichs, *Theor. Chem. Acc.* **1997**, *97*, 119–124.
[45] E. R. Davidson, *J. Chem. Phys.* **1967**, *46*, 3320–3326.
[46] K. R. Roby, *Mol. Phys.* **1974**, *27*, 81–87.
[47] R. Heinzmann, R. Ahlrichs, *Theor. Chim. Acta* **1976**, *42*, 33–37.
[48] C. Ehrhardt, R. Ahlrichs, *Theor. Chim. Acta* **1985**, *68*, 231–240.
[49] F. Jensen, *Introduction to Computational Chemistry*, Wiley, Chichester, England, **1999**.
[50] A. Klamnt, *J. Phys. Chem.* **1995**, *99*, 2224–2235; A. Klamnt *J. Phys. Chem.* **1996**, *100*, 3349–3353.

Received: May 6, 2004
Published online: December 2, 2004